Transport in topologically disordered one-particle, tight-binding models

Abdellah Khodja,[*] Hendrik Niemeyer,[†] and Jochen Gemmer[‡]
Fachbereich Physik, Universität Osnabrück, Barbarastrasse 7, D-49069 Osnabrück, Germany
(Received 21 December 2012; revised manuscript received 1 March 2013; published 28 May 2013)

We aim at quantitatively determining transport parameters like conductivity, mean free path, etc., for simple models of spatially completely disordered quantum systems, comparable to the systems which are sometimes referred to as Lifshitz models. While some low-energy eigenstates in such models always show Anderson localization, we focus on models for which most states of the full spectrum are delocalized, i.e., on the metallic regime. For the latter we determine transport parameters in the limit of high temperatures and low fillings using linear response theory. The Einstein relation (proportionality of conductivity and diffusion coefficient) is addressed numerically and analytically and found to hold. Furthermore, we find the transport behavior for some models to be in accord with a Boltzmann equation, i.e., rather long mean free paths, exponentially decaying currents, while this does not apply to other models even though they are also almost completely delocalized.

DOI: 10.1103/PhysRevE.87.052133 PACS number(s): 05.60.Gg, 72.80.Ng, 66.30.Ma

I. INTRODUCTION

A large part of electronic transport theory on disordered systems is based on spatially ordered, periodic crystal structures to which disordered impurities, distortions, on-site potentials, etc., are added. As long as the effect of these disordered addends is weak, transport analysis may be performed by mapping the electronic dynamics onto a Boltzmann equation in which the Bloch states of the periodic part of the model correspond to free particles. This concept has been rigorously derived in Ref. [1] and quantitatively applied in, e.g., Refs. [2–5]. Whenever the influence of the disordered part becomes large the execution of this approach becomes challenging [2]. Quantitative results on transport in strongly disordered 3D, one-particle quantum systems appear to be rare, some results on the Anderson model have been reported in Refs. [6–8]. In the paper at hand transport theory is approached from the opposite side: We consider models which do not feature any spatially ordered structure whatsoever, and this model class is sometimes referred to as "Lifshitz models." We do not focus on weak random potentials but start from tight-binding models, the sites of which are spatially distributed completely at random. This is incorporated into the quantum models by means of distance-dependent hopping terms in the tight-binding model. We find that reliable results on transport properties of such extended, 3D, disordered models in the high-temperature limit may be obtained using standard linear response theory and numerically exact diagonalization of finite samples comprising about 17 000 sites.

The investigation at hand addresses transport in substantially disordered systems but within the delocalized energy regime (i.e., no thermally activated hopping transport within the localized regime), thus, the models cannot be viewed as models for, say, transport in real amorphous silicon [9]. The discussed type of transport may occur in strongly doped but weakly compensated semiconductors or amorphous metals. However, rather than modeling realistic systems in great detail, we focus on more general features of the transport dynamics. While the accepted picture appears to be that transport phenomena within the delocalized regime in disordered systems may generally be described using a Drude or Boltzmann approach [10], we find that this is not necessarily the case. Close to the Anderson transition there appears to be a regime in which the electrons are already delocalized but their transpoprt dynamics seems to be incompatible with a Boltzmann equation.

The paper at hand is organized as follows: After introducing our models in Sec. II we identify delocalized regimes in those in Sec. III. This analysis is not meant to be an exhaustive and detailed investigation of localization in Lifshitz models, it only serves to identify the regime in which quantitative transport investigations may reasonably be performed. In Sec. IV the conductivity at high temperatures and low fillings for a variety of models is numerically computed on the basis of linear response theory. Diffusion coefficient and Einstein relation are addressed, both analytically and numerically, in Sec. V. Some features of the above findings on transport behavior indicate that the models exhibit two different types of transport behavior even in the delocalized regimes: "Boltzmann transport" and "non-Boltzmann transport." This finding is worked out in some detail in Sec. VI through consideration of a mean free path. We close with a summary and conclusion in Sec. VII.

II. TOPOLOGICALLY DISORDERED TIGHT-BINDING MODELS

The models we investigate are three-dimensional, one-particle tight-binding models. The sites at which the particle may be found, however, are not located periodically in space; rather, are they distributed completely at random. Such models have been thoroughly investigated for spectral properties, etc., by Lifshitz [11]. However, while the focus there is on the density of states and the transition from the localized to the metallic regime, we focus on transport within the metallic regime. The finite samples of these models on which our investigations are based are generated as follows: A cube of volume $L^3 = N$ in real space is defined. Then a set

[*]akhodja@uos.de
[†]hniemeye@uos.de
[‡]jgemmer@uos.de

of N position vectors $\vec{x}_j$ are drawn at random by drawing each coordinate of each vector independently from a uniform distribution on the interval $[0,L]$. This guarantees a uniform site distribution with unit density. Now a tight-binding model with hopping or orbital overlap terms is defined as

$$\hat{H} = \sum_{jk} H_{jk} \hat{a}_j^\dagger \hat{a}_k, \tag{1}$$

where $\hat{a}_i^\dagger, \hat{a}_i$ denotes the annihilation and creation operators. The function H_{jk} describes the dependence of the overlap terms on the positions of the respective sites. We consider isotropic overlap, thus, H_{jk} essentially depends on the distance between site j and site k. Generally we assume H_{jk} to be decreasing with increasing site distances; however, the overlap terms will not be limited to nearest neighbors. Since we impose periodic boundary conditions (eventually in order to keep finite-size effects as small as possible) the distance s_{jk} is a somewhat complex function. It may be defined as

$$s_{jk} := \sqrt{d_{jk}^2(x) + d_{jk}^2(y) + d_{jk}^2(z)}, \tag{2}$$

where the d' are essentially the Cartesian components of $(\vec{x}_j - \vec{x}_k)$. Due to periodic boundary conditions, they are now defined as

$$d_{jk}(\alpha) = \begin{cases} |\alpha_j - \alpha_k|, & |\alpha_j - \alpha_k| < \frac{L}{2} \\ L - |\alpha_j - \alpha_k|, & |\alpha_j - \alpha_k| > \frac{L}{2} \end{cases}, \tag{3}$$

where α is one of the Cartesian coordinates, i.e., $\alpha = x,y,z$. Thus, the distance s_{jk} is essentially the shortest distance between the sites j,k under periodic closure of the sample. With this definition of the distance we now specify three model types as follows.

Model type I: The overlap terms as entering the Hamiltonian in (1) are taken to decrease exponentially with the distance, i.e.,

$$H_{jk}^{\mathrm{I}} := \exp\left(\frac{-3 s_{jk}}{\tilde{l}}\right), \tag{4}$$

where $\tilde{l}$ is a parameter that equals the mean overlap length, i.e., this and all following overlap terms are constructed such that

$$\frac{1}{N} \sum_{jk} s_{jk} \left| H_{jk}^{\mathrm{I,II,III}} \right| = \tilde{l}. \tag{5}$$

This specific model type has been chosen since its Anderson transition with respect to $\tilde{l}$ has been discussed in the literature and, thus, the corresponding value $\tilde{l} \approx 0.6$ is fairly well known, cf. Ref. [12] and references therein. (Note that the definition of the parameter that controls the overlap length in Ref. [12] differs slightly from the one at hand.) However, as will become clear below, it is particularly difficult to obtain quantitative results on transport behavior for this specific model type. Thus, we introduce another model type for which results are much less affected by finite-size effects.

Model type II: Here we define the overlap terms as decreasing as a Gaussian with the distance, i.e.,

$$H_{jk}^{\mathrm{II}} := \exp\left(\frac{-4 s_{jk}^2}{\pi \tilde{l}^2}\right) \tag{6}$$

again the function is constructed in such a way that (5) holds. This model is interesting since it shows, as will become clear below, a transition from transport behavior comparable to Brownian motion (non-Boltzmann transport) to transport dynamics as occurring in a crystal with some impurities (Boltzmann transport) with increasing $\tilde{l}$. It turns out that this transition only occurs if the phases of the overlap terms are nonrandom. In order to demonstrate this we investigate a third type.

Model type III: Here we also define the absolute values of the overlap terms as decreasing as a Gaussian with the distance; however, we allow for random phases

$$H_{jk}^{\mathrm{III}} := \exp\left(\frac{-4 s_{jk}^2}{\pi \tilde{l}^2} + i \phi_{jk}\right), \tag{7}$$

where the ϕ_{jk}, for say, $j > k$ are real random numbers drawn independently from the interval $[0,2\pi]$. Of course, to guarantee hermiticity of the Hamiltonian the ϕ_{kj} have then to be chosen as $\phi_{kj} = -\phi_{jk}$. This leaves the absolute values unchanged such that (5) still holds. In some sense this model is even more random than model type I and model type II and, as it turns out, shows non-Boltzmann transport only.

All above models but especially model type III bare a similarity with the "banded random matrix models" as discussed in, e.g., Ref. [13], in which the overlap terms that connect sites below a certain distance are simply chosen at random, all other overlap terms are set to zero. In Ref. [13] it is reported that those models exhibit diffusive behavior in 3D on a relevant time scale if the characteristic overlap length is sufficiently long. Although the models at hand differ somewhat, our results are in principle in accord with the findings in Ref. [13].

The above models are all isotropic, i.e., the hopping amplitudes depend on the distance of the respective sites only. This, however is no crucial prerequisite for all the below investigations. Anisotropic disordered systems like, e.g., discussed in Ref. [14] may be analyzed in the same way.

III. DETECTION OF DELOCALIZED REGIMES AS A BASIS FOR TRANSPORT INVESTIGATIONS

The main focus of the paper at hand is the quantitative analysis of macroscopic transport properties of the above-defined models (cf. Sec. II). However, as we are dealing with disordered models Anderson localization may occur which affects the transport properties severely. Localized states are basically energy eigenstates that feature spatial probability distributions with finite spreads, even if the model is infinitely large. For a given 3D model at a given energy the eigenstates are either localized or extended. Usually the delocalized states are in the center of the spectrum (or the bands) while localization occurs at the edges [8,15,16]. If some model parameter, e.g., the magnitude of disordered on-site potentials, hopping lengths, etc., is tuned in some direction the localized part of the spectrum may increase such that at some point all states are localized (Anderson transition). If the parameter is tuned to the opposite extreme it is expected that (in 3D) in the limit practically all states at all energies

become delocalized [8]. At an energy regime at which states are localized all macroscopic transport coefficients such as diffusion constant, conductivity, etc., vanish, i.e., the system behaves as an isolator on the large scale (this refers to the isolated system, i.e., no phonon-assisted, thermally activated transport like discussed, e.g., in Ref. [9] is considered here). In the work at hand we are interested in the transport behavior of the delocalized regime only. In order to make sure that the changes in transport behavior with model parameters which we investigate below are not simply due to the onset of localization we first aim at finding models and parameter regimes which are almost completely delocalized. To this end we have to consider the spectrum and the delocalized part of it. The precise determination of the mobility edge (precise energy which seperates localized from delocalized regimes) is a formidable task of its own. In the context of the Anderson model it has been approached by sophisticated techniques such as transfer matrix methods, Thouless scaling, fractal analysis, etc. [16,17]. For our purposes it suffices to have less precise information on the mobility edge since we only intend to find out whether the biggest part of the spectrum is delocalized. Thus, we employ a rather simple criterion to determine the approximate position of the mobility edge. This criterion is based on the inverse participation number

$$I(E) := \sum_{i=1}^{N} |\psi(E,i)|^4. \tag{8}$$

Here $\psi(E,i)$ is the amplitude at site i of an energy eigenstate with energy E. Localization analysis based on the inverse participation number is well established. It has been used even for rather detailed investigations in the Anderson model [17], as well as for topologically disordered systems [18]. Here we suggest a very simple "delocalization indicating criterion": we guess that states at an energy E are surely delocalized if $I(E) < 90/N$ for a finite but large-enough model of size N. This guess appears to be in reasonable accord with various more carefully derived results on the mobility edge from the literature. It has furthermore the advantage of being numerically cheap since it turns out that averaging over about five random models described by the same model parameters suffices to identify $E_{\text{deloc.}}$ from $I(E_{\text{deloc.}}) = 90/N$ with reasonable accuracy. We find (as expected) that this equation has two solutions; thus, the regime between those two energies is delocalized.

We illustrate our "delocalization criterion" in Figs. 1, 2, and 3, which refer to the model types I, II and III, respectively. The figures show a "scaled inverse participation number," i.e., $NI(E)$ as a function of E for various N together with the density of states (DOS), given in arbitrary units. (If not mentioned otherwise all data presented in this paper are averaged over five random implementations of the addressed model as defined in Sec. II. However, this averaging appears not to be crucial, typically the data for various implementations of the same model looks very similar. Wherever the data are presented as a histogram of course a further averaging over an appropriate bin size is performed.)

Figures 1(a), 2(a), and 3(a) correspond to mean overlap lengths $\tilde{l}$ which are only very slightly above the Anderson

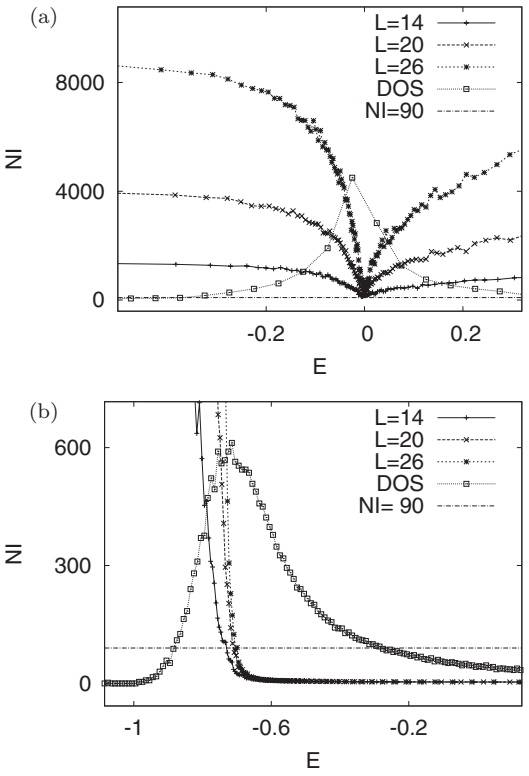

FIG. 1. Scaled inverse participation number $NI(E)$ and density of states (DOS) for model type I. (a) Corresponds to mean overlap length $\tilde{l} = 0.6$ which appears to be at the Anderson transition; (b) corresponds to mean overlap length $\tilde{l} = 4$; an extended delocalized regime appears to exist.

transition. Accordingly, the regime in which the $NI(E)$ coincide is very narrow and appears to yield $NI(E) \approx 90$. The value for Fig. 1(a) is in very good agreement with results on the Anderson transition for the same model reported in Ref. [12] and references therein. Figures 1(b), 2(b), and 3(b) correspond to mean overlap lengths $\tilde{l}$ substantially above the Anderson transition. Correspondingly, there are extended regimes to which $NI(E) \leqslant 90$ applies. Furthermore, for large-enough N the scaled inverse participation numbers to which $NI(E) \leqslant 90$ applies appear to become independent of N which indicates that states within this regime are indeed delocalized. For some models and some energies we additionally computed the mobility edge from the more costly method described in Ref. [17]. It turns out that the deviations between the so-computed mobility edge and our $E_{\text{deloc.}}$ are on the order of 5%. As final demostration of the validity of our delocalization criterion, we compare the energies at which $NI(E) = 90$ for the 3D Anderson models with results on the mobility edge from the literature [19,20]. (Note that this is only to "calibrate" our criterion, i.e., determine the factor "90." We will not analyze the Anderson model quantitatively for transport; such an investigation may be found in Ref. [21].) The results are shown in Fig. 4. Obviously there is reasonable agreement between result from our criterion and data from the literature. The agreement appears to become better in the regime we are interested in, i.e., disorders W where most of the eigenstates are delocalized.

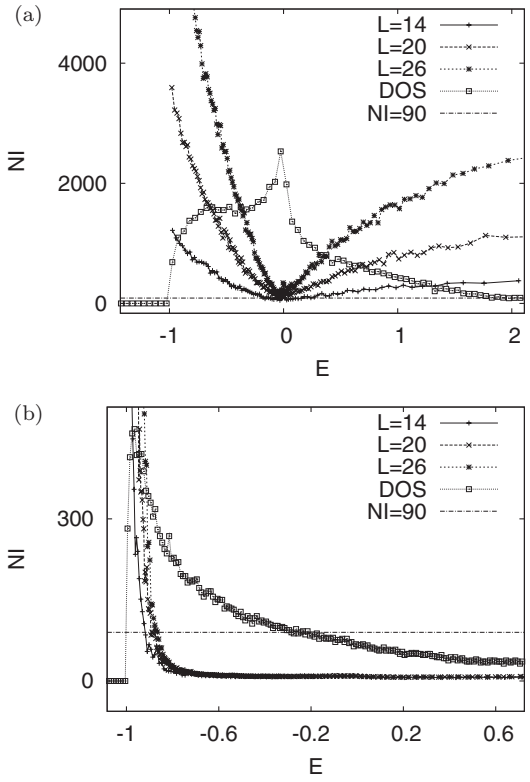

FIG. 2. Scaled inverse participation number $NI(E)$ and density of states (DOS) for model type II. (a) Corresponds to mean overlap length $\tilde{l} = 0.7$ which appears to be at the Anderson transition; (b) corresponds to mean overlap length $\tilde{l} = 1$; an extended delocalized regime appears to exist.

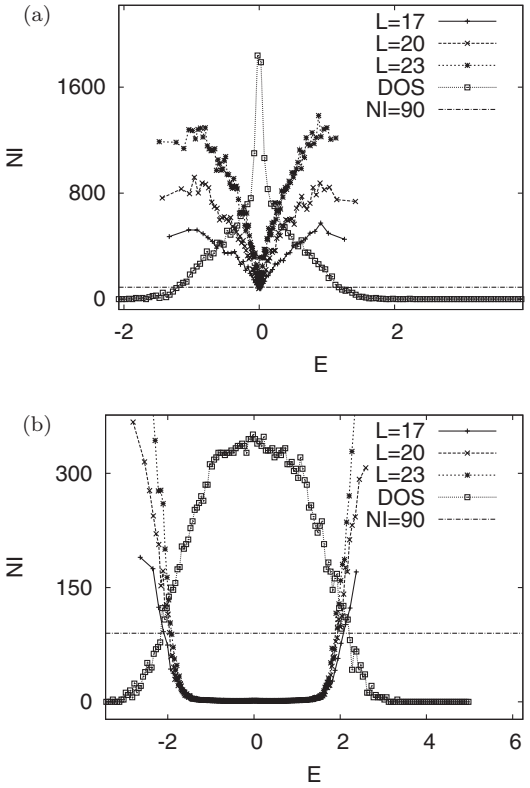

FIG. 3. Scaled inverse participation number $NI(E)$ and density of states (DOS) for model type III. (a) Corresponds to mean overlap length $\tilde{l} = 0.6$ which appears to be at the Anderson transition; (b) corresponds to mean overlap length $\tilde{l} = 1$; an extended delocalized regime appears to exist.

Our method is not appropriate to determine the Anderson transition or the mobility edges with great precision because $NI(E_c)$ in the critical region is not a constant but depends on the sample size (fractal dimension). It, however, appears well suited to quickly identify models for which the vast majority of all energy eigenstates is delocalized which is the purpose of the investigation at hand. It may be worth noting here that frequently, e.g., in the context of the Anderson model, the mobility edge lies in an energy regime with a relatively low density of states. This, however, appears to hold for the present models only for type III. For model types I and II the mobility edge appears to lie at or close to the maximum density of states, cf. Figs. 1(b), 2(b), and 3(b). After those preliminary considerations we now simply calculate the percentage of all energy eigenstates for which $NI(E) \leqslant 90$, according to the previous considerations we expect this to be close to or a little smaller then the percentage of all eigenstates that are delocalized. This is done for all three model types and various mean overlap lengths. The result is displayed in Fig. 5. Obviously, the Anderson transition for all three model types occurs, very roughly, around $\tilde{l} \approx 0.6$. However, whereas for model types II and III almost all states are delocalized for $\tilde{l} \geqslant 1.3$ [Fig. 5(b)] a substantial fraction of states remains localized up to $\tilde{l} \approx 6$ for model-type I [Fig. 5(a)]. Since it is a reasonable assumption that, using numerical diagonalization, reliable transport constants may only be obtained for sample sizes that are large compared to the mean overlap length, we do not pursue the analysis of model type I any further for we are numerically limited to sample sizes of $L = 26$.

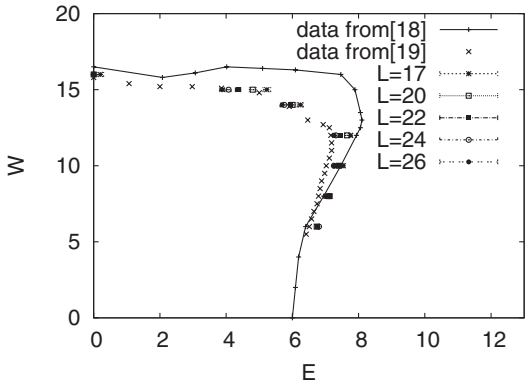

FIG. 4. Results on the mobility edge in the 3D Anderson model; W quantifies the degree of disorder. Compared are results from the "$90/N$" criterion for different sample sizes to results from more refined methods from the literature [19,20]. The results from our $90/N$ criterion appear to converge reasonably against the results from Ref. [20]. Error bars for the $90/N$ criterion indicate variations arising from different random implementations of the Anderson model featuring the same degree of disorder.

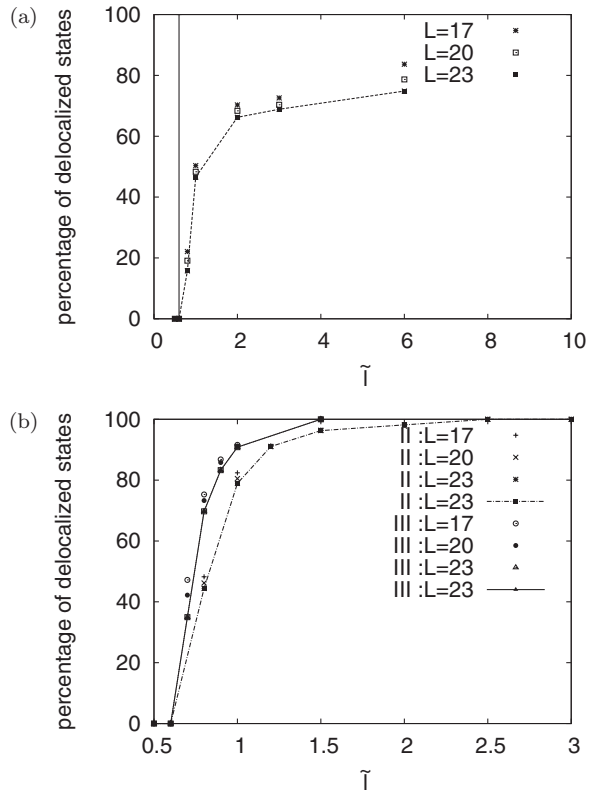

FIG. 5. Percentage of delocalized energy eigenstates for various mean overlap lengths $\tilde{l}$. Panel (a) addresses model type I. The vertical solid line at $\tilde{l} = 0.6$ indicates the Anderson transition as found in Ref. [12]. Although the data appear not to be fully converged for some $\tilde{l}$ it is obvious that about 30% of the spectrum remain localized up to $\tilde{l} = 6$. Panel (b) addresses model types II and III. Although the data appear not to be fully converged for some $\tilde{l}$ close to the Anderson transition, it is obvious that less than 10% (and decreasing) of the spectrum are localized for $\tilde{l} > 1.3$.

IV. CONDUCTIVITY AT LOW FILLINGS AND HIGH TEMPERATURES

First, we investigate the conductivity of model types II and III for various hopping lengths. We employ linear response theory, i.e., the Kubo formula. In the limit of high temperatures and low fillings (routinely described within the framework of the grand-canonical ensemble) the dc conductivity is given as

$$\sigma_{\mathrm{dc}} = \sigma(t \to \infty), \quad \sigma(t) = \frac{f}{T}\int_0^t \frac{1}{N}\,\mathrm{Tr}\,\{\hat{J}(t')\hat{J}(0)\}dt' \tag{9}$$

[22,23], where f is the filling factor (mean number of particles per site at equilibrium), N denotes the number of sites in the sample (since we work at unit spatial site density N also equals the volume), trace and current operators refer to the one-particle sector only, and, furthermore, $J(t)$ denotes the current operator in the Heisenberg picture. T is the temperature and we set $k_B = 1, \hbar = 1$, and, furthermore, we set the charges of the particles to unity, i.e., $q = 1$. Now, of course, an appropriate current operator has to be defined. In the context of periodic systems this is often done by considerations based on the continuity equation for the particle density [24–27]. Here we choose a definition of the current which is based on the "velocity" in, say, x direction, i.e.,

$$\hat{v} = i[\hat{H}, \hat{x}]. \tag{10}$$

Here $\hat{x}$ is a x-position operator and it is defined as

$$\hat{x} = \sum_{i=1}^{N} x_i \hat{n}_i, \quad \hat{n}_i := \hat{a}_i^\dagger \hat{a}_i, \tag{11}$$

where x_i is the x coordinate of the position of site i. Thus, the operator $\hat{v}$ may also be written as

$$\hat{v} = i\sum_{ij}(x_j - x_i)H_{ij}\hat{a}_i^\dagger \hat{a}_j. \tag{12}$$

The interpretation of such an operator as velocity or current is somewhat in conflict with periodic boundary conditions (which we impose for technical reasons). A (slow) transition of probability from, say, the right edge of the sample ($x = L$) to the left edge of the sample ($x = 0$) would give rise to very high negative velocities. But within the concept of periodic boundary conditions such a transition should correspond to low positive velocities. Thus, in order to obtain a suitable current operator, we modify the above velocity operator (12) such that it features the same structure for transitions arising from the periodic closure as it already exhibits for transitions within the sample,

$$\hat{J} = \sum_{ij} J_{ij}\hat{a}_i^\dagger \hat{a}_j$$

$$J_{ij} = \begin{cases} i[x_j - x_i]H_{ij} & |x_j - x_i| < \frac{L}{2} \\ \mathrm{sgn}(x_j - x_i)[i[L - |x_j - x_i|]H_{ij}] & |x_j - x_i| > \frac{L}{2} \end{cases}. \tag{13}$$

Equipped with this definition for the current we may now simply calculate the current autocorrelation function as appearing in (9). We do so using standard numerically exact diagonalization routines. Within reasonable computing time we are able to treat samples up to a size of $L = 26$. It turns out that this appears to be sufficient to render finite-size effects for a range of models negligible. In order to be able to compare the key features of the dynamics of the current autocorrelation functions for various model types and sizes to each other we compute a kind of "normalized" current autocorrelation functions, $j'(t) := \mathrm{Tr}\{\hat{J}(t)\hat{J}(0)\}/\mathrm{Tr}\{\hat{J}^2(0)\}$.

Figures 6(a) and 6(b) show $j'(t)$ for model types II and III for different sample sizes. Obviously the $j'(t)$ coincide for the larger sample sizes for the relevant times, i.e., for times at which $j'(t)$ is substantially different from zero. From this finding we conclude that in this case finite-size effects are indeed negligible. However, whether or not $L = 26$ is sufficient to get rid of finite-size effects depends on the model type and the mean overlap length. Typically, finite-size effects are less severe for shorter mean overlap lengths. Figure 7(a) shows $j'(t)$ for model type II ($L = 26$) for two mean overlap lengths. $\tilde{l} = 1.3$ is the shortest mean overlap length for which most likely the largest part of the spectrum is still delocalized [cf. Fig. 5(b)], and $\tilde{l} = 2.2$ is the longest mean overlap length for which we obtain results that are reliably unaffected by

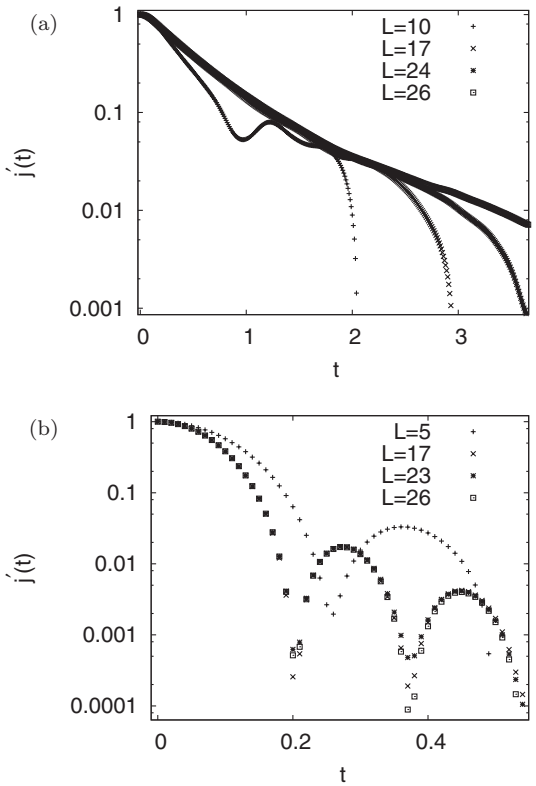

FIG. 6. Normalized current autocorrelation function $j'(t)$ for increasing sample sizes L. Note that due to the logarithmic scale the initial dynamics is most relevant. Panel (a) addresses model-type II, with mean overlap length $\tilde{l} = 2.0$. The data appear to be reasonably free of finite-size effects for $L \geqslant 24$. The decay appears to be essentially exponential. Panel (b) addresses model type III, with mean overlap length $\tilde{l} = 4.0$. The data appears to be reasonably free of finite-size effects for $L \geqslant 17$. The decay appears to be essentially Gaussian

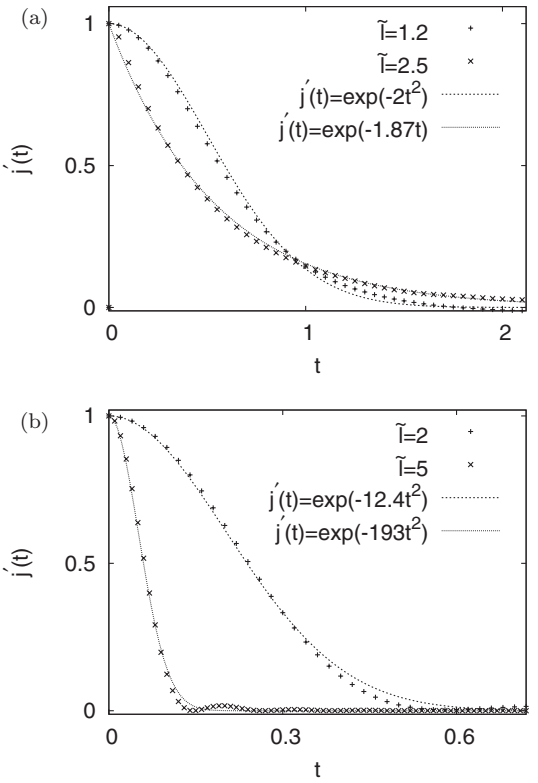

FIG. 7. Normalized current autocorrelation function $j'(t)$ for the longest and shortest reasonable mean overlap lengths $\tilde{l}$ (see text), sample size $L = 26$. Panel (a) addresses model type II, with mean overlap length $\tilde{l} = 1.2$ and $\tilde{l} = 2.5$. The decay appears to be dominantly Gaussian for the short and dominantly exponential for the long mean overlap lengths. Panel (b) addresses model type III, with mean overlap lengths $\tilde{l} = 2.0$ and $\tilde{l} = 5.0$. The decay appears to be essentially Gaussian for both mean overlap lengths.

finite-size effects. Figure 7(b) shows $j'(t)$ for model type III for an intermediate mean overlap length. For model type II the relaxation dynamics appear to undergo a transition from a Gaussian decay to an exponential decay as the mean overlap lengths become larger, cf. Fig. 7(a). For model type III the relaxation dynamics are more or less Gaussian at all mean overlap lengths, cf. Fig. 7(b). The exponential decay of the current for model type II at long mean overlap lengths suggests that the respective dynamics may be interpreted as the dynamics of almost free (lattice) particles which are only weakly scattered [23]. Within the framework of such and interpretation the (disordered) eigenstates of the current operator $\hat{J}$ take the role of the Bloch states in a periodic crystal. Since such a behavior may be described on a phenomenological level by a Boltzmann equation we call this type of dynamics "Boltzmann transport." For all cases in which the current decays nonexponentially (e.g., Gaussian) the dynamics cannot be described by a standard Boltzmann equation, this occurs although this cases correspond to the metallic (delocalized) regime as well. Thus, we call this type of dynamics "non-Boltzmann transport." We elaborate on this issue in more detail ins Sec. VI. To conclude the considerations on conductivity we plot $\sigma_{\mathrm{dc}} f/T$ for model types II and III over mean overlap length (on a double logarithmic scale); see Fig. 8. The plot clearly suggests a power-law scaling of the conductivity mean overlap length. The corresponding fits yield, for the respective conductivities,

$$\sigma_{\mathrm{dc}}^{\mathrm{II}} = \frac{f}{T} 0.17\ \tilde{l}^{4.83}, \quad \sigma_{\mathrm{dc}}^{\mathrm{III}} = \frac{f}{T} 0.19\ \tilde{l}^{3.54}. \tag{14}$$

This scaling is considered to be valid only in a certain regime. On one side, the regime is limited by $\tilde{l} \geqslant 1.3$, since below that value substantial parts of the spectrum become localized, which is, of course, expected to change transport behavior drastically. On the other side, this scaling is not necessarily believed to hold arbitrarily far from the critical point. Our numerics, however, indicate that it holds within the regime displayed in the figures. This is our first main quantitative result. While the conductivities of the two model types appear to coincide at $\tilde{l} \approx 1.3$ the conductivity increases much faster with increasing mean overlap lengths in model type II. This supports the concept of model type II exhibiting Boltzmann-transport for longer mean overlap lengths, while model type III always shows non-Boltzmann transport.

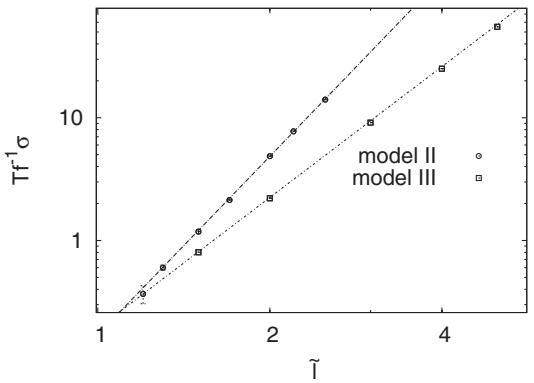

FIG. 8. Scaled conductivity $Tf^{-1}\sigma_{dc}$ (or diffusion constant D, see text) for model types II and III as a function of mean overlap length $\tilde{l}$, with sample size $L = 26$. For both model types the conductivity appears to scale as a power law with $\tilde{l}$; the dashed (− − −, model type II) and dotted (. . ., model type II) lines are the respective fits, cf. (14). Whereas at $\tilde{l} \approx 1.3$ the conductivities more or less coincide the conductivity for model type II appears to increase much faster. The vertical error bars correspond to different random implementations of the same model.

V. DIFFUSION CONSTANT AND EINSTEIN RELATION

Apart from the conductivity the diffusion coefficient is another important transport quantity. According to the Einstein relation, conductivity and the diffusion constant should be proportional to each other. However, the validity of the Einstein relation and the limits of its applicability have been much debated subjects and continue to be so in the context of quantum systems [28] (and references therein). Recently it has been reported that the Einstein relation holds for periodic, interacting, 1D quantum systems at high temperatures. It is claimed to hold even for finite times, thus taking the form [28]

$$D(t) = \frac{T}{\epsilon^2}\sigma(t), \tag{15}$$

where $D(t)$ is the (time-dependent) diffusion constant and ϵ^2 is the uncertainty (variance) of the transported quantity per site at the respective equilibrium. In the following we investigate whether this relation also holds for the disordered, noninteracting, 3D quantum systems at hand. In our case the transported quantity is the particle density. In the limit of high temperatures and low fillings the equilibrium fluctuations scale as $\epsilon^2 = f$ [22]. Thus, if one hypothetically accepts the validity of (15) also for the system at at hand, one gets from inserting (9)

$$D(t) = \int_0^t \frac{1}{N}\mathrm{Tr}\{\hat{J}(t')\hat{J}(0)\}dt'. \tag{16}$$

In the following we demonstrate that almost the same relation between the diffusion constant and the current autocorrelation function may also be obtained from another consideration which applies to the disordered systems at hand. If a diffusion equation holds, the derivative with respect to time of the spatial variance of the diffusing quantity equals twice the diffusion constant [28]. We may analyze the dynamics of this variance on quantum mechanical grounds for the models hat hand. If initially the particle is completely concentrated at site i and we assume that the spatial expectation value does not move (which is an assumption since the model is disordered, but since the disorder is isotropic the assumption appears reasonable and furthermore may be justified by numerical checking) the variance $\delta^2 x_i(t)$ reads

$$\delta^2 x_i(t) = \sum_j (x_j - x_i)^2 \mathrm{Tr}\{\hat{n}_j(t)\hat{n}_i\}. \tag{17}$$

Averaging this over all sites yields

$$\Delta^2 x(t) = \frac{1}{N}\sum_{ij}(x_j - x_i)^2 \mathrm{Tr}\{\hat{n}_j(t)\hat{n}_i\}. \tag{18}$$

Taking the second derivative with respect to time yields

$$\frac{d^2}{dt^2}\Delta^2 x(t) = -\frac{1}{N}\sum_{ij}(x_j - x_i)^2 \mathrm{Tr}\{[\hat{H},[\hat{H},\hat{n}_j(t)]]\hat{n}_i\}. \tag{19}$$

Due to the invariance of the trace under cyclic permutation of the traced operators this may be rewritten as

$$\frac{d^2}{dt^2}\Delta^2 x(t) = \frac{1}{N}\sum_{ij}(x_j - x_i)^2 \mathrm{Tr}\{[\hat{H},\hat{n}_j(t)][\hat{H},\hat{n}_i]\}. \tag{20}$$

Since the total particle number $\sum_i \hat{n}_i(t)$ is conserved, the respective commutators vanish and the remainder reads

$$\frac{d^2}{dt^2}\Delta^2 x(t) = \frac{-2}{N}\sum_{ij}\mathrm{Tr}\{[\hat{H},x_j\hat{n}_j(t)][\hat{H},x_i\hat{n}_i]\}. \tag{21}$$

This, however, is essentially the velocity autocorrelation function, cf. (10) and (11), such that

$$\frac{d^2}{dt^2}\Delta^2 x(t) = \frac{2}{N}\mathrm{Tr}\{\hat{v}(t)\hat{v}(0)\}. \tag{22}$$

Given that, as explained above, $\frac{d}{dt}\Delta^2 x(t) = 2D(t)$ we get

$$D(t) = \int_0^t \frac{1}{N}\mathrm{Tr}\{\hat{v}(t')\hat{v}(0)\}dt'. \tag{23}$$

Which is, up to the difference between $\hat{v}$ and $\hat{J}$, the same relation one also gets from boldly applying an Einstein relation that has been derived in a different context, cf. (16). The difference between $\hat{v}$ and $\hat{J}$ is not completely trivial since the periodic boundary conditions change the topology of the system. Nevertheless, (16) and (23) encourage a numerical check of the validity of the Einstein relation for the systems at hand in the respective sense. This numerical check proceeds as follows: We implement an initial state of the form

$$\rho(0) = \frac{1}{Z}\exp\left[-\frac{\left(\hat{x} - \frac{L}{2}\right)^2}{2}\right],$$
$$Z = \mathrm{Tr}\left\{\exp\left[-\frac{\left(\hat{x} - \frac{L}{2}\right)^2}{2}\right]\right\}, \tag{24}$$

i.e., a state in which the probability is more or less concentrated in a thin slab of a thickness on the order of 1, perpendicular to the x axis in the middle of the cubic sample. We calculate the increase of the variance of this state and take a derivative with respect to time,

$$D_1(t) = \frac{1}{2}\frac{d}{dt}\mathrm{Tr}\{\hat{x}^2(t)\rho(0)\}. \tag{25}$$

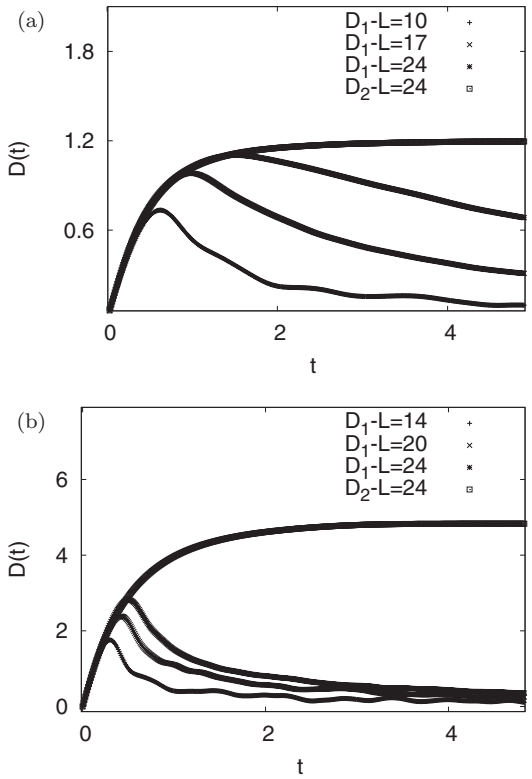

FIG. 9. Comparison of two methods to calculate (time-dependent) diffusion coefficients: $D_1(t)$ from (25) and $D_2(t)$ from (26). The data address model type II with (a) mean overlap length $\tilde{l} = 1.5$ and (b) mean overlap length $\tilde{l} = 2.0$ for the indicated sample sizes. Obviously, finite-size effects are more pronounced for $D_1(t)$; however, it appears to converge against $D_2(t)$ for large sample sizes. This coincidence implies the validity of an Einstein relation.

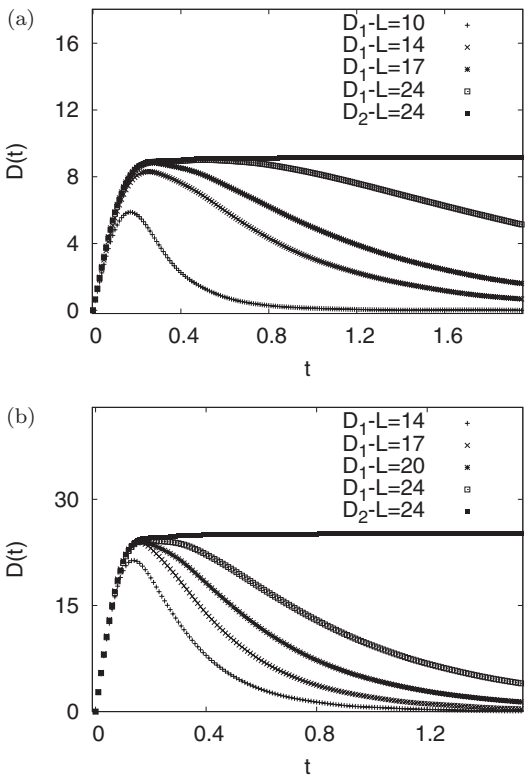

FIG. 10. Comparison of two methods to calculate (time-dependent) diffusion coefficients: $D_1(t)$ from (25) and $D_2(t)$ from (26). The data address model type III with (a) mean overlap length $\tilde{l} = 3.0$ and (b) mean overlap length $\tilde{l} = 4.0$ for the indicated sample sizes. Obviously, finite-size effects are more pronounced for $D_1(t)$; however, it appears to converge against $D_2(t)$ for large sample sizes. This coincidence implies the validity of an Einstein relation

This corresponds to the diffusion constant one obtains from monitoring the spatial expansion of the probability distribution. We compare this to the integrated current autocorrelation function, which is what (16) and (23) imply:

$$D_2(t) = \int_0^t \frac{1}{N} \mathrm{Tr}\{\hat{J}(t')\hat{J}(0)\} dt'. \tag{26}$$

The results are displayed in Figs. 9 and 10 for model types II and III. Although finite-size effects are much more pronounced if the diffusion constant is calculated by means of (25), there is, for the initial, valid time period a very good agreement in the sense of (15). Thus, we conclude that the Einstein relation is valid for the systems at hand and Fig. 8 may be viewed as not only describing the conductivity but also the diffusion constant at high temperatures.

VI. DIFFERENT TYPES OF TRANSPORT BEHAVIOR: BOLTZMANN AND NON-BOLTZMANN TRANSPORT

As already indicated in Sec. IV, it appears reasonable to interpret the described transport behavior in terms of two different transport types, although both correspond to the metallic regime: Non-Boltzmann transport which is (in a sense described below) comparable to the dynamics of an overdamped Brownian particle or the thermally activated hopping transport which may occur in the localized regime of amorphous and/or doped semiconductors [9] and Boltzmann transport which resembles the dynamics of a particle in a periodic lattice featuring some impurities or a system of quasifree, weakly interacting particles. These transport types have also been found in other one-particle quantum systems, e.g., non-Boltzmann transport in modular quantum systems [29,30] and both transport-types in the 3D Anderson model [6,17]. In order to elaborate on this point somewhat further we define a "mean free path" for the models at hand from the following consideration: If the particle was completely ballistic (infinite mean free path) the current autocorrelation function would never decay and the time-dependent diffusion coefficients in the sense of (16) would always increase linearly. The time-dependent diffusion coefficients of the models at hand increase linearly at the beginning, cf. Figs. 9 and 10, but reach a final plateau after that initial period. We define, somewhat arbitrarily, the ballistic period as the period before the diffusion coefficient has reached 90% of its eventual value. Now we call the mean free path the square root of the increase of the spatial variance of an initial state of type (24) during this ballistic period. So the mean free path is roughly the initial increase of width of an initially narrow probability distribution up to the point where the fully diffusive dynamics begins. The so-defined mean free paths λ are displayed in Fig. 11. The

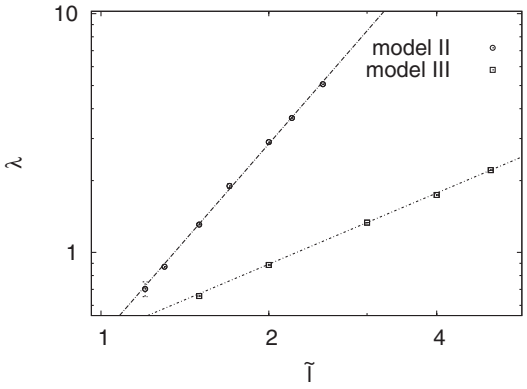

FIG. 11. Mean free paths λ (for definition see text) for model types II and III as a function of mean overlap length $\tilde{l}$, sample size $L = 26$. For both model types the mean free paths appear to scale as power laws with $\tilde{l}$; the dashed (− − −, model type II) and dotted (. . ., model type III) lines are the respective fits, cf. (27). While for model type III the mean free path is always lower than the mean overlap length $\lambda_{\mathrm{III}} < \tilde{l}$ the mean free path of model type II becomes larger than the mean overlap length $\tilde{l}$ at about $\tilde{l} \approx 1.8$. This indicates that model type II undergoes a transition from non-Boltzmann to Boltzmann transport, while model type III does not. The vertical error bars correspond to different random implementations of the same model. These variations appear to increase for small $\tilde{l}$.

mean free path appears to scale as a power law with the mean overlap length for both model types II and III. The respective fits yield

$$\lambda_{\mathrm{II}} = 0.44\ \tilde{l}^{2.68}, \quad \lambda_{\mathrm{III}} = 0.45\ \tilde{l}^{0.99}. \tag{27}$$

As already mentioned below (14) this scaling is considered to be valid only in a certain regime. On one side the regime is limited by $\tilde{l} \geqslant 1.3$, since below that value substantial parts of the spectrum become localized, which is of course expected to change transport behavior drastically. On the other side, this scaling is not necessarily believed to hold arbitrarily far from the critical point. Our numerics, however, indicate that it holds within the regime displayed in the figures.

This is our second main quantitative result. While the mean free paths of the two model-types are very similar for $\tilde{l} \approx 1.3$ [cf. Fig. 5(b)], the mean free path increases much faster with increasing hopping lengths in model type II. This finding supports the classification of the two different types of transport: While for model type III the mean free path λ remains below and scales as the mean overlap length for all $\tilde{l}$, it appears that λ becomes larger than $\tilde{l}$ for mean overlap lengths above, say, $\tilde{l} \approx 1.8$ for model type II. Thus, transport in model type III may always be classified as non-Boltzmann transport, whereas the transport behavior of model type II appears to undergo a transition from non-Boltzmann to Boltzmann transport at about $\tilde{l} \approx 1.8$. This point of view is, furthermore, supported by the fact that the current autocorrelation function decays in Gaussian fashion at all $\tilde{l}$ for model type III, whereas it undergoes a transition from Gaussian to exponential decay for model type II at $\tilde{l} \approx 1.8$, cf. Fig. 7(a). Note that this Boltzmann transport occurs, although model II is also topologically completely disordered, i.e., features no site order whatsoever.

VII. SUMMARY AND CONCLUSION

We investigated the transport behavior of quantum systems which may be described as three-dimensional, topologically completely disordered, one-particle, tight-binding models on the basis of the Schroedinger equation. These models are intended as very simplified descriptions of (hypothetical) solids in which the atomic nuclei are distributed completely at random in space without any short- or long-range order. The hopping or orbital overlap terms of the tight-binding Hamiltonian are simply taken to be decreasing functions of the distances between the nuclei. By means of a simple method based on the inverse participation number, we identify (rather roughly) the localized regimes. While the Anderson transition appears to occur approximately at a mean overlap length of $\tilde{l} \approx 0.6$ (with respect to the mean site distance) for all considered models, some models exhibit delocalized eigenstates at more or less all energies already at mean overlap lengths of $\tilde{l} > 1.3$ in others 30% of the spectrum remain localized up to mean overlap lengths of $\tilde{l} > 6$. For quantitative transport investigations we focused on models which are almost entirely delocalized. The conductivity at low fillings and high temperatures has been determined by evaluating the Kubo formula using numerically exact diagonalization for finite samples. It turns out that valid quantitative results with negligible finite size effects may be obtained for a range of models at sample sizes of about 17 000 sites. The conductivities are found to depend as power laws on the mean overlap lengths sufficiently above the Anderson transition. In addition to the conductivity also the diffusion coefficient is addressed. Theoretical considerations which suggest that an Einstein relation should hold, i.e., that the diffusion coefficient may expected to be proportional to the conductivity are presented. Those considerations are numerically confirmed by monitoring the expansion of an initially narrow wave package. Eventually a mean free path is defined and numerically determined. It is found that for a range of models the mean free path substantially exceeds the mean overlap length. This suggests that these models may be thought of as systems in which particles travel almost ballistically over distances much larger than the typical site distance and undergo only weak scattering, like in the case of a periodic crystal containing some impurities. This holds although the systems feature no spatial order whatsoever.

[1] L. Erdős, M. Salmhofer, and H. Yau, Acta Math. **200**, 211 (2008).
[2] I. Mertig, E. Mrosan, and P. Ziesche, *Multiple Scattering Theory of Point Defects in Metals: Electronic Properties*, Teubner-Texte zur Physik, Vol. 11 (Leipzig, 1987).
[3] J. P. Dekker, A. Lodder, and J. van Ek, Phys. Rev. B **57**, 12719 (1998).
[4] N. Papanikolaou, N. Stefanou, and C. Papastaikoudis, Phys. Rev. B **49**, 16117 (1994).

[5] T. Vojta, I. Mertig, and R. Zeller, Phys. Rev. B **46**, 15761 (1992).
[6] R. Steinigeweg, H. Niemeyer, and J. Gemmer, New J. Phys. **12**, 113001 (2010).
[7] P. Markos, Acta Phys. Slovaka **56**, 561 (2006).
[8] B. Kramer and A. MacKinnon, Rep. Prog. Phys. **56**, 1469 (1993).
[9] B. I. Shklovskii and A. L. Efros, *Electronic Properties of Doped Semiconductors* (Springer, Berlin, 1984).
[10] B. L. Altshuler and A. G. Aronov, *Electron–Electron Interactions in Disordered Systems,* edited by A. L. Efros and M. Pollak (Elsevier, Amsterdam, 1985).
[11] I. M. Lifshitz, Adv. Phys. **13**, 483 (1964).
[12] J. D. Bauer, V. Logovinsky, and J. L. Skinner, J. Phys. C: Solid State Phys. **21**, 993 (1988).
[13] L. Erdős and A. Knowles, Comm. Math. Phys. **303**, 509 (2011).
[14] A. Rodriguez, A. Chakrabarti, and R. A. Romer, Phys. Rev. B **86**, 085119 (2012).
[15] S. Knief, W. von Niessen, and T. Koslowski, Phys. Rev. B **58**, 4459 (1998).
[16] *50 Years of Anderson Localization*, edited by E. Abrahams (World Scientific, Singapore, 2010).
[17] J. Brndiar and P. Markos, Phys. Rev. B **74**, 153103 (2006).
[18] R. Atta-Fynn, P. Biswas, P. Ordejon, and D. A. Drabold, Phys. Rev. B **69**, 085207 (2004).
[19] H. Grussbach and M. Schreiber, Phys. Rev. B **51**, 663 (1995).
[20] B. Bulka, M. Schreiber, and B. Kramer, Z. Phys. B **66**, 21 (1987).
[21] R. Steinigeweg, J. Gemmer, H.-P. Breuer, and H.-J. Schmidt, Eur. Phys. J. B **69**, 275 (2009).
[22] R. Kubo, M. Toda, and N. Hashitsume, *Statistical Physics II: Nonequilibrium Statistical Mechanics* (Springer, Berlin, 1991).
[23] J. Jaeckle, *Einführung in die Transporttheorie* (Vieweg, Braunschweig, 1978).
[24] X. Zotos, Phys. Rev. Lett. **82**, 1764 (1999).
[25] F. Heidrich-Meisner, A. Honecker, D. C. Cabra, and W. Brenig, Phys. Rev. B **68**, 134436 (2003).
[26] J. Benz, T. Fukui, and A. K. C. Scheeren, J. Phys. Soc. Jpn. Suppl. **74** (2005).
[27] J. Gemmer, R. Steinigeweg, and M. Michel, Phys. Rev. B **73**, 104302 (2006).
[28] R. Steinigeweg, H. Wichterich, and J. Gemmer, Europhys. Lett. **88**, 10004 (2009).
[29] R. L. Weaver, Phys. Rev. E **73**, 036610 (2006).
[30] M. Michel, G. Mahler, and J. Gemmer, Phys. Rev. Lett. **95**, 180602 (2005).